Design for broadband on-chip isolator using stimulated Brillouin scattering in dispersion-engineered chalcogenide waveguides

Christopher G. Poulton,[1,2,*] **Ravi Pant,**[1,3] **Adam Byrnes,**[1,3] **Shanhui Fan,**[1,3,4] **M. J. Steel,**[1,5] **and Benjamin J. Eggleton**[1,3]

[1]*Centre for Ultrahigh bandwidth Devices for Optical Systems (CUDOS), Australia*
[2]*School of Mathematical Sciences, University of Technology, Sydney, (UTS), Sydney, NSW 2007, Australia*
[3]*School of Physics, University of Sydney, Sydney, NSW 2006, Australia*
[4]*Department of Electrical Engineering, Stanford University, Stanford, California 94305, USA*
[5]*MQ Photonics Research Centre, Department of Physics and Astronomy, Macquarie University, Sydney, NSW 2109, Australia*

[*]*chris.poulton@uts.edu.au*

Abstract: We propose a scheme for on-chip isolation in chalcogenide (As_2S_3) rib waveguides, in which Stimulated Brillouin Scattering is used to induce non-reciprocal mode conversion within a multi-moded waveguide. The design exploits the idea that a chalcogenide rib buried in a silica matrix acts as waveguide for both light and sound, and can also be designed to be multi-moded for both optical and acoustic waves. The enhanced opto-acoustic coupling allows significant isolation ($>$ 20 dB) within a chip-scale (cm-long) device ($<$ 10 cm). We also show that the bandwidth of this device can be dramatically increased by tuning the dispersion of the waveguide to match the group velocity between optical modes: we find that 20 dB isolation can be extended over a bandwidth of 25 nm.

OCIS codes: (190.0190) Nonlinear optics; (190.2640) Stimulated scattering, modulation, etc.; (190.4360) Nonlinear optics, devices.

References and links

1. M. Soljacić and J. D. Joannopoulos, "Enhancement of nonlinear effects using photonic crystals." Nat. Mater. **3**, 211–219 (2004).
2. X. Huang and S. Fan, "Complete all-optical silica fiber isolator via Stimulated Brillouin Scattering," J. Lightwave Technol. **29**, 2267–2275 (2011).
3. Z. Yu and S. Fan, "Complete optical isolation created by indirect interband photonic transitions," Nat. Photonics **3**, 91–94 (2009).
4. Z. Yu and S. Fan, "Integrated nonmagnetic optical isolators based on photonic transitions," IEEE J. Sel. Top. Quantum Electron. **16**, 459–466 (2010).
5. L. J. Aplet and J. W. Carson, "A Faraday effect optical isolator," Appl. Optics **3**, 544–545 (1964).
6. M. Levy, "The on-chip integration of magnetooptic waveguide isolators," IEEE J. Sel. Top. Quantum Electron. **8**, 1300–1306 (2002).
7. Y. Shoji, T. Mizumoto, H. Yokoi, I. Hsieh, and R. Osgood, "Magneto-optical isolator with silicon waveguides fabricated by direct bonding," Appl. Phys. Lett. **92**, 071117 (2008).
8. M.-C. Tien, T. Mizumoto, P. Pintus, H. Kroemer, and J. Bowers, "Silicon ring isolators with bonded nonreciprocal magneto-optic garnets," Opt. Express **19**, 11740–11745 (2011).

#172916 - $15.00 USD Received 20 Jul 2012; revised 21 Aug 2012; accepted 21 Aug 2012; published 31 Aug 2012

9. K. Gallo and G. Assanto, "All-optical diode based on second-harmonic generation in an asymmetric waveguide," J. Opt. Soc. Am. B **16**, 267–269 (1999).
10. L. Fan, J. Wang, L. T. Varghese, H. Shen, B. Niu, Y. Xuan, A. M. Weiner, and M. Qi, "An all-silicon passive optical diode." Science **335**, 447–450 (2012).
11. M. Fujii, A. Maitra, C. Poulton, J. Leuthold, and W. Freude, "Non-reciprocal transmission and Schmitt trigger operation in strongly modulated asymmetric WBGs," Opt. Express **14**, 12782–12793 (2006).
12. H. Lira, Z. Yu, S. Fan, and M. Lipson, "Electrically driven nonreciprocity induced by interband photonic transition on a silicon chip," Phys. Rev. Lett. **109**, 033901 (2012).
13. R. W. Boyd, *Nonlinear optics*, 3rd ed. (Academic Press, 2003).
14. M. S. Kang, A. Butsch, and P. S. J. Russell, "Reconfigurable light-driven opto-acoustic isolators in photonic crystal fibre," Nat. Photonics **5**, 549–553 (2011).
15. B. J. Eggleton, B. Luther-Davies, and K. Richardson, "Chalcogenide photonics," Nat. Photonics **5**, 141–148 (2011).
16. R. Pant, C. G. Poulton, D.-Y. Choi, H. Mcfarlane, S. Hile, E. Li, L. Thevenaz, B. Luther-Davies, S. J. Madden, and B. J. Eggleton, "On-chip stimulated Brillouin scattering." Opt. Express **19**, 8285–8290 (2011).
17. R. Pant, E. Li, D.-Y. Choi, C. G. Poulton, S. J. Madden, B. Luther-Davies, and B. J. Eggleton, "Cavity enhanced stimulated Brillouin scattering in an optical chip for multiorder Stokes generation," Opt. Lett. **36**, 3687–3689 (2011).
18. J. D. Love and N. Riesen, "Single-, Few-, and Multimode Y-Junctions," J. Lightwave Technol. **30**, 304–309 (2012).
19. L. B. Soldano and E. C. M. Pennings, "Optical multi-mode interference devices based on self-imaging: principles and applications," J. Lightwave Technol. **13**, 615–627 (1995).
20. B. A. Auld, *Acoustic Fields and Waves in Solids, Volume II*, 1st ed. (John Wiley & Sons, 1973).
21. P. Rakich, C. Reinke, R. Camacho, P. Davids, and Z. Wang, "Giant enhancement of stimulated Brillouin scattering in the subwavelength Limit," Phys. Rev. X **2**, 1–15 (2012).
22. K. Finsterbusch, N. J. Baker, V. G. Ta'eed, B. J. Eggleton, D.-Y. Choi, S. Madden, and B. Luther-Davies, "Higher-order mode grating devices in As2S3 chalcogenide glass rib waveguides," J. Opt. Soc. Am. B **24**, 1283–1290 (2007).
23. R. Pant, A. Byrnes, C. G. Poulton, E. Li, D.-y. Choi, S. Madden, B. Luther-davies, and B. J. Eggleton, "Photonic-chip-based tunable slow and fast light via stimulated Brillouin scattering," Opt. Lett. **37**, 969–971 (2012).
24. J. Goell, "A circular-harmonic computer analysis of rectangular dielectric waveguides," Bell Syst. Tech. J. **48**, 2133–2160 (1969).
25. N. Uchida and N. Niizeki, "Acoustooptic Deflection Materials and Techniques," Proc. IEEE **61**, 1073–1092 (1973).
26. S. Ramachandran, Z. Wang, and M. Yan, "Bandwidth control of long-period grating-based mode converters in few-mode fibers," Opt. Lett. **27**, 698–700 (2002).
27. M. W. Lee, C. Grillet, S. Tomljenovic-Hanic, E. C. Mägi, D. J. Moss, B. J. Eggleton, X. Gai, S. Madden, D.-Y. Choi, D. A. P. Bulla, and B. Luther-Davies, "Photowritten high-Q cavities in two-dimensional chalcogenide glass photonic crystals," Opt. Lett. **34**, 3671–3673 (2009).
28. M. Shokooh-Saremi, V. G. Ta, N. J. Baker, I. C. M. Littler, D. J. Moss, B. J. Eggleton, Y. Ruan, and B. Luther-Davies, "High-performance Bragg gratings in chalcogenide rib waveguides written with a modified Sagnac interferometer," J. Opt. Soc. Am. B **23**, 1323–1331 (2006).

1. Introduction

Optical isolation, whereby light is permitted to propagate in one direction but not in the other, is an important capability for modern photonics devices [1–4]. Traditionally, isolation is achieved using the non-reciprocity of Faraday rotation in magneto-optic materials [5], and there has been much recent research that focuses on the incorporation of magnetic elements on a chip-scale device [6–8]. To complement this magneto-optic approach, a number of researchers have proposed alternative isolation schemes that make use of the non-reciprocal nature of optical nonlinearities [9] in conjunction with resonators [10] and strongly modulated gratings [11], or that create non-reciprocity by direct temporal modulation of the material properties of a waveguiding material [3,4,12]. A flexible, chip-based isolation scheme that is capable of linear operation over a range of wavelengths would be a powerful and useful addition to the range of components available for modern integrated photonics.

We present here a scheme for all-optical isolation based on Stimulated Brillouin Scattering (SBS) in highly-nonlinear chalcogenide (As_2S_3) rib waveguides. SBS is one of the strongest op-

#172916 - $15.00 USD Received 20 Jul 2012; revised 21 Aug 2012; accepted 21 Aug 2012; published 31 Aug 2012

tical nonlinearities, and involves a coherent interaction between the optical and acoustic modes within the material [13]. The central idea for an SBS-based isolator, first proposed in a fibre geometry [2], is that two optical pumps are used to generate an acoustic field in a waveguide via electrostriction; the density fluctuations in the acoustic mode then induce a travelling photo-elastic grating which causes optical signals in the co-propagating direction to undergo mode-conversion, while signals travelling in the counter-propagating direction are unaffected. This scheme leads to operation that is independent of the power in the signal, and offers a broader bandwidth of isolation than alternative SBS-based isolation schemes [14], in which the signal itself generates the acoustic field.

The original proposal for an SBS-based isolation scheme [2] required 12 m of small-diameter (1.34 μm) fibre suspended in air for effective operation. We demonstrate here that this scheme can be extended to practical on-chip operation. An essential component to the operation of this device is the use of highly-nonlinear chalcogenide waveguides [15]. These waveguides have two key advantages for use in SBS experiments: firstly, the high refractive index leads to a large Brillouin gain, some 100$\times$ that of a silica waveguide with equivalent dimensions [16,17]. Secondly, the material properties of chalcogenide are such that a waveguide can be formed for both acoustic and optical waves using a buried As_2S_3 waveguide in silica [16]. This conveys a significant advantage over free-standing or suspended waveguides.

The structure of the paper is as follows. First, we outline the principles of operation of the device. We then examine the acoustic properties of chalcogenide rib waveguides and outline how the fields are computed. Design curves are then presented showing the range of operation, for realistic pump powers, of the isolation scheme. Finally, we show that the bandwidth of the device can be markedly increased by tailoring the dispersion of the multi-mode waveguide.

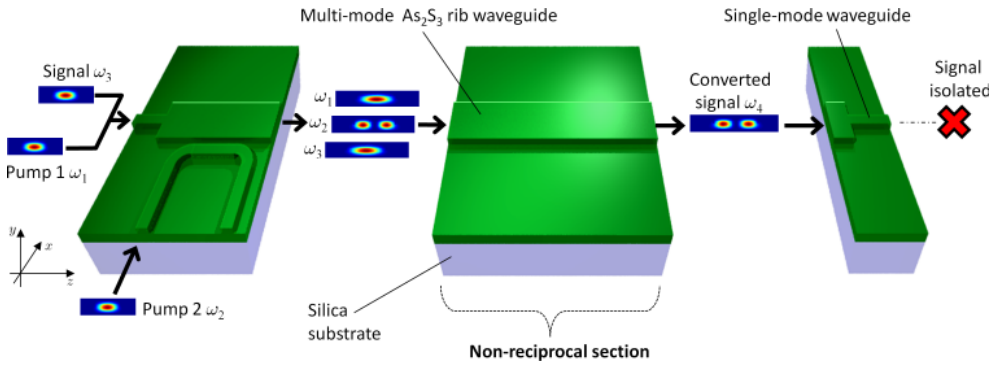

Fig. 1. Schematic of isolator operation. Two pump modes are mixed into the fundamental and first higher-order mode of a multi-mode chalcogenide rib waveguide. These pumps excite a guided acoustic mode in the long central section, which drives a transition from the signal in the fundamental mode at ω_3 to a higher-order mode at frequency ω_4. The higher-order mode is then filtered out using symmetry. A signal propagating in the reverse direction does not undergo mode conversion, and so can propagate from the right to the left of the device unimpeded except for losses at the waveguide transitions.

2. Principal of operation and theory

We consider the device shown in Fig. 1. Two CW pump sources at frequencies ω_1 and ω_2 are mixed by a mode coupler [18,19] into the fundamental and higher-order optical modes, respectively, of a multi-mode rib waveguide. These modes have propagation constants β_1 and β_2, and should be sufficiently far from cutoff that their dispersion curves are very nearly parallel (see

#172916 - $15.00 USD Received 20 Jul 2012; revised 21 Aug 2012; accepted 21 Aug 2012; published 31 Aug 2012

Fig. 2(a)). The beat pattern between these two modes will then excite density fluctuations with frequency $\Omega = \omega_2 - \omega_1$ and propagation constant $q = \beta_2 - \beta_1$ via electrostriction; if the pair (q, Ω) lies on the dispersion curve of an acoustic mode then the acoustic mode will be resonantly excited by the optical fields. The acoustic field will drive inter-band transitions between the forward-propagating fundamental and higher-order optical modes over a large bandwidth: as shown in Fig. 2(a), a forward-propagating signal in the fundamental optical mode at frequency ω_3 will interact with the acoustic wave via the elasto-optic effect to form a higher-order optical mode with frequency $\omega_4 = \omega_3 + \Omega$. For a signal travelling in the reverse direction this transition is not possible as there is no optical mode that fulfills the required energy-momentum conservation – the rib waveguide therefore acts as a non-reciprocal mode converter. The higher-order mode at ω_4 can then be filtered out, for example by exploiting the difference in symmetry between the modes. For the anti-symmetric higher-order mode depicted in Fig. 1, a simple transition to a single-mode waveguide can be used as a mode filter. Because of symmetry, the overlap between the higher-order optical mode and the fundamental mode of a narrow waveguide is exactly zero, however the higher-order mode is beyond cut-off in the narrow waveguide and so cannot propagate further.

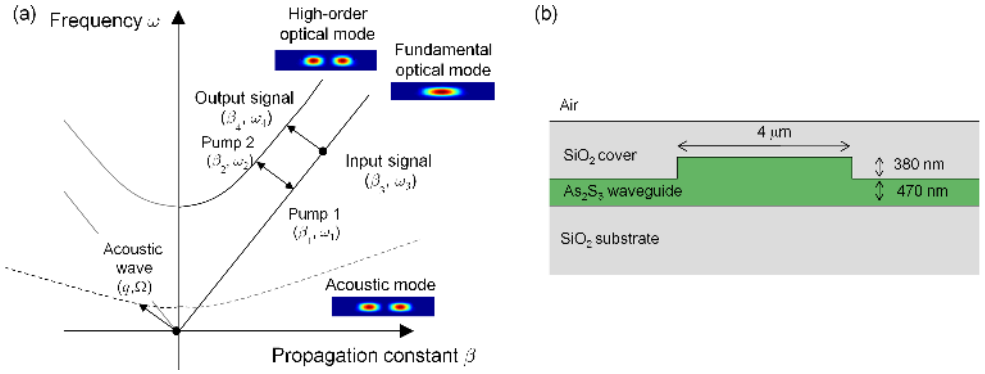

Fig. 2. (a) Dispersion diagram showing the optical and acoustic modes: energy and momentum conservation must be satisfied to drive the transition from one optical mode to another; (b) Rib waveguide design used in our simulations.

The isolation attainable in such a device depends on the degree of mode conversion in the multi-mode rib, which in turn depends on the interaction between optical and acoustic fields over the length of the waveguide. This interaction can be modeled using coupled-mode theory, and we now give an outline of the formalism, following for the most part the more comprehensive derivation of Huang and Fan [2]. In the interaction there are four optical fields, consisting of two pumps (at ω_1 and ω_2) and two signals (at ω_3 and ω_4). For a waveguide oriented along the z-axis, the electric fields of each mode can be expanded:

$$\mathbf{E}_k(x,y,z,t) = a_k(z,t)\mathbf{e}_k(x,y)e^{i(\beta_k z - \omega_k t)} + \text{c.c}\ . \tag{1}$$

Here the (three-dimensional) vector $\mathbf{e}_k$ represents the electric field of the k^{th} mode with frequency ω_k and propagation constant β_k, and $a_k(z,t)$ is an envelope function, which is assumed to be slowly varying in both time and in the z-direction. For the following analysis we normalize each optical mode so that $\int\int_A ||\mathbf{e}_k||^2 \mathrm{d}x\mathrm{d}y = 1$, where the integral extends over the waveguide cross-section. The corresponding expansion for the acoustic field is

$$\rho(x,y,z,t) = b(z,t)\rho_{\text{ac}}(x,y)e^{i(qz - \Omega t)} + \text{c.c}\ . \tag{2}$$

#172916 - $15.00 USD Received 20 Jul 2012; revised 21 Aug 2012; accepted 21 Aug 2012; published 31 Aug 2012

where $b(z,t)$ is a slowly-varying function that describes the acoustic field envelope along the waveguide. The function $\rho_{\rm ac}$ describes the dilatation of the acoustic mode, which satisfies the wave equation [20]

$$\nabla_\perp^2 \rho_{\rm ac} + (\frac{\Omega_{\rm ac}^2}{V_{\rm ac}^2} - q^2)\rho_{\rm ac} = 0 \,, \tag{3}$$

where $V_{\rm ac}(x,y)$ is the longitudinal acoustic velocity in the material and $\Omega_{\rm ac}$ is the angular frequency of the acoustic mode with wavenumber q. In writing Eq. (3) we have assumed that the major part of the acoustic field consists of pressure waves and that contributions from shear waves can be neglected. This choice is valid in situations where the dominant coupling mechanism is electrostriction and where the waveguide is far enough from cutoff that effects from radiation pressure can be neglected [21]. The appropriate boundary conditions to be applied for Eq. (3) are then continuity of the value of $\rho_\perp$ across material boundaries, together with homogeneous Dirichlet conditions on those surfaces where the solid material boundary connects with a gaseous or vacuum boundary [20]. We additionally apply homogeneous Dirichlet conditions on the edge of the computational domain in the x direction, and choose this domain large enough that the acoustic mode is not affected by this boundary. With these boundary conditions, Eq. (3) becomes a well-posed eigenvalue problem for the acoustic modes. We normalize these modes by setting $\int\int_A |\rho_{\rm ac}|^2 {\rm d}x{\rm d}y = 1$.

By substituting the expansions (1) into Maxwell's equations and Eq. (2) into Eq. (3), applying the mode normalizations, and taking into account the slow-varying behavior of the envelopes, we obtain the coupled amplitude equations for the acoustic field $b(z)$ and the optical modes $a_k(z)$. In deriving these equations, other nonlinear effects are neglected because the pumps and signals are CW [2, 13]. We choose the frequencies of the pump modes ω_1 and ω_2 to exactly match the zero-detuning point from the SBS resonance, so that $\omega_2 - \omega_1 = \Omega_a$ and $\beta_2 - \beta_1 = q$. This is the most efficient operating point for the generation of phonons, and at this point we obtain the steady-state solution for the acoustic field:

$$b(z) \quad = \quad \varepsilon_0 Q_{12}'' a_1^*(z) a_2(z) \,, \tag{4}$$

with the coupled amplitude equations for the pump modes:

$$\frac{{\rm d}a_1}{{\rm d}z} = \frac{i\omega_1 Q_{12}}{2n_1 c(1-K_1)} a_2 b^* \,, \quad \frac{{\rm d}a_2}{{\rm d}z} = \frac{i\omega_2 Q_{21}}{2n_2 c(1-K_2)} a_1 b \,. \tag{5}$$

In the above equations, $n_{1,2}$ denotes the effective index of modes 1 and 2, and the coefficients Q_{12}, Q_{12}'' and $K_{1,2}$ are overlap integrals defined by:

$$Q_{ij} \quad = \quad \iint_A \frac{\gamma_e}{\rho_0} \, \mathbf{e}_i \cdot \mathbf{e}_j^* \, \rho_{\rm ac}^* {\rm d}x \, {\rm d}y \,, \quad Q_{ij}'' = \iint_A \frac{\gamma_e}{\Gamma_B} \, \nabla^2 \left(\mathbf{e}_i \cdot \mathbf{e}_j^* \right) \, \rho_{\rm ac}^* {\rm d}x \, {\rm d}y \,, \tag{6}$$

$$K_j \quad = \quad \iint_A |[\mathbf{e}_j]_z|^2 + \frac{1}{2i\beta_j} \left([\mathbf{e}_j]_z^* \nabla_\perp \cdot [\mathbf{e}_j]_\perp + [\mathbf{e}_j]_\perp^* \cdot \nabla_\perp [\mathbf{e}_j]_z \right) {\rm d}x \, {\rm d}y \,. \tag{7}$$

Here $\gamma_e(x,y)$ is the local coefficient of electrostriction [13] of the waveguide material, that is, the coefficient of the material at position (x,y). $\rho_0(x,y)$ is the material density at equilibrium, and $\Gamma_B(x,y)$ is the intrinsic Brillouin linewidth [13] of a bulk solid consisting entirely of the material at position (x,y). We use $\nabla_\perp$ and $[\mathbf{e}_j]_\perp$ to denote projections onto the transverse (x,y) plane.

The acoustic field generated by the two pumps creates a grating via the elasto-optic effect, resulting in coupling between the signals located at frequencies ω_3 and ω_4. At this point we depart from the treatment in [2], and note that in general the difference in the signal modes will be detuned by an amount $\Delta\beta = q - (\beta_2 - \beta_1)$ from the centre of the Brillouin resonance.

#172916 - $15.00 USD Received 20 Jul 2012; revised 21 Aug 2012; accepted 21 Aug 2012; published 31 Aug 2012

Assuming that the signals are much smaller in amplitude than either of the pump modes, the coupled amplitude equations for the signal modes are then

$$\frac{da_3}{dz} = \frac{i\omega_3 Q_{34}}{2n_3 c(1-K_3)} e^{-i\Delta\beta z} a_4 b^* \ , \quad \frac{da_4}{dz} = \frac{i\omega_4 Q_{43}}{2n_4 c(1-K_4)} e^{i\Delta\beta z} a_3 b \ . \tag{8}$$

The two coupled sets of equations (4)-(5) and (8) can be solved numerically to determine the power carried by the signal modes, and hence to compute the degree of mode conversion along the waveguide. The "raw" optical isolation, that is, the isolation achievable provided the modes can be perfectly filtered, is then given by

$$I_{\mathrm{dB}} = 10\log_{10}\left(\frac{P_3(z=z_{\max})}{P_3(z=0)}\right) \ , \tag{9}$$

where $z_{\max}$ is the length of the waveguide and $P_k(z)$ denotes the power carried by the k^{th} mode, given by

$$P_k = 2\varepsilon_0 n_k c |a_k|^2 \iint_A \mathbf{e}_k \times \mathbf{h}_k^* \mathrm{d}x \, \mathrm{d}y \ .$$

3. Acoustic and optical modes in chalcogenide rib waveguides

Before solving Eq. (4-5) and Eq. (8) we must determine the nature of the acoustic and electromagnetic modes that exist within the guide. To achieve maximum conversion of the signal from the fundamental mode at ω_3 to a higher order mode at ω_4 several requirements must be satisfied. First, the optical modes must be of the same or similar polarization, to ensure that the quantity $\mathbf{e}_1 \cdot \mathbf{e}_2^*$ is non-zero. The symmetry of the acoustic mode must also be appropriate for driving the inter-band transition, and there should be significant overlap with the optical field intensity – acoustic modes of the wrong symmetry will result in the coupling integrals Q_{ij} and Q''_{ij} being equal to zero. In addition, it is desirable that the quantity $\Delta\beta$ be as small as possible, so as to match momentum between the acoustic field and the transition between the signal modes. These considerations mean that the waveguide must not only be multi-moded but also that the modes must have a very similar group velocity extending over as large a bandwidth as possible. This means that the modes should be sufficiently far from cut-off that the waveguide dispersion is very small.

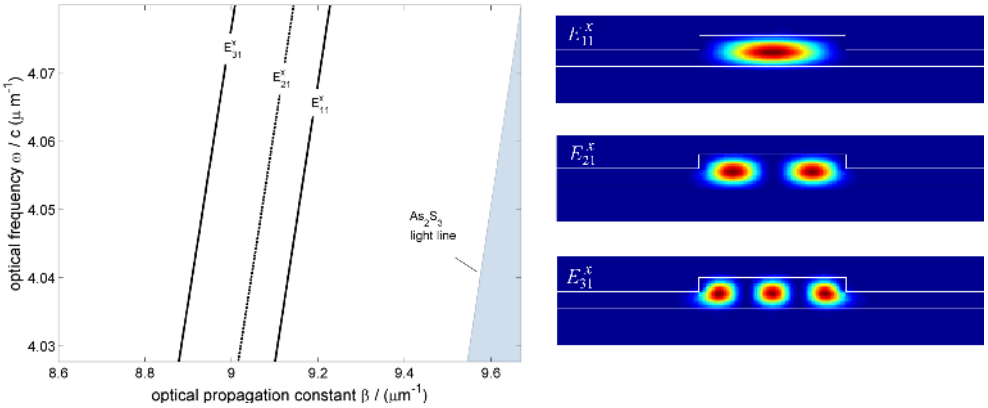

Fig. 3. Electromagnetic modes for the rib waveguide depicted in Fig. 2(b): the z-component of the time-averaged Poynting vector is depicted.

With these factors in mind we consider a waveguide geometry that has previously been shown to exhibit strong Brillouin response – the chalcogenide rib waveguide (see Fig. 2(b)). These

#172916 - $15.00 USD Received 20 Jul 2012; revised 21 Aug 2012; accepted 21 Aug 2012; published 31 Aug 2012

waveguides are also multi-moded [22] provided that we choose a sufficiently wide rib; in the following we choose a rib of width 4 μm with a height of 380 nm on a slab with thickness 470 nm, placed on a silica substrate and covered completely with a silica coating. These dimensions have been chosen because they have previously been demonstrated as practical for on-chip SBS-based experiments [16, 17, 23], with reasonable insertion loss ($\sim$ 4dB per facet) and moderate waveguide losses $\sim$ 0.2dB/cm [23]. Optimization of the waveguide parameters to increase the device bandwidth is considered in Section 5. In principle it is possible to remove the Silica coating and still achieve confinement of both optical and acoustic fields, however in practice it is desirable to have some protective covering over the light-guiding rib to reduce losses. In the vicinity of $\lambda = 1550$ nm the rib has a refractive index of $n_{As_2S_3} = 2.37$, while the substrate has a refractive index of $n_{SiO_2} = 1.44$. In Fig. 3 we show the dispersion curves of the TE-like modes, which possess a dominant electric field component oriented along the x-axis, for this waveguide geometry. Several modes, displaying both odd and even symmetry, are available in this frequency range; following the classification of Goell and others [24] we consider the E^x_{11} (even), E^x_{21} (odd) and E^x_{31} (even) modes.

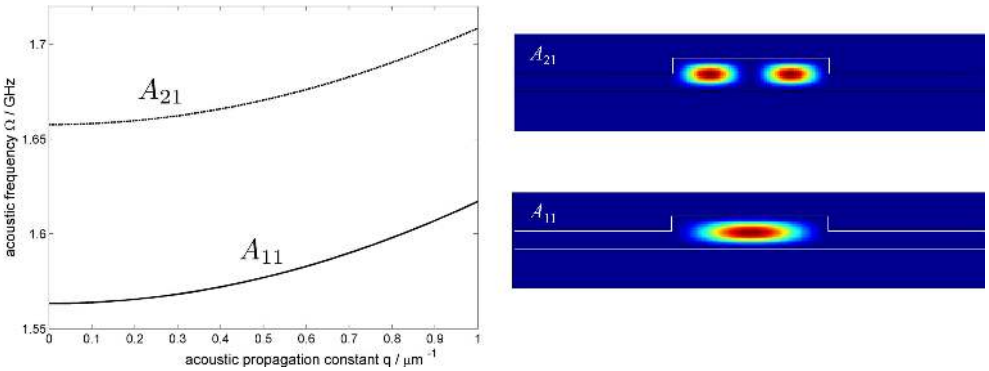

Fig. 4. Fundamental and first higher-order acoustic modes for the rib waveguide depicted in Fig. 2(b). The normalized acoustic energy density is depicted.

This structure also supports several acoustic modes. These are computed by directly solving Eq. (3) using the finite element package COMSOL, together with the appropriate boundary conditions. The local velocities of sounds were chosen to be $v_{As_2S_3} = 2600$ m s^{-1} and $v_{SiO2} = 5971$ ms^{-1}, with material densities $\rho_{As_2S_3} = 3198$ kg m^{-3}, $\rho_{SiO_2} = 2200$ kg m^{-3} [25]. The acoustic modes are guided within the chalcogenide material because the acoustic wave, like an electromagnetic wave, will be confined within the region where the phase velocity is lowest. This means that simultaneous confinement of optical and acoustic waves is possible without having to use under-etched membranes [21] or multi-structured optical fibres [14]. The dispersion curves for small values of wavenumber q are shown in Fig. 4. Following the nomenclature for optical modes, we designate the acoustic modes A_{11}, A_{21}, A_{31}, with the indices designating the number of antinodes in the x and y directions respectively.

4. Isolation and power-dependence

There are two possibilities for mode conversion in this structure involving the fundamental E^x_{11} mode: The E^x_{11} mode could interact with an even acoustic mode (such as A_{11}) to produce an even optical mode (such as E^x_{31}). The second possibility is that E^x_{11} could interact with an odd acoustic mode (A_{21}) to produce an odd optical mode (E^x_{21}). There is always a larger overlap between field components for the even-odd interaction, and therefore this interaction will be

#172916 - $15.00 USD Received 20 Jul 2012; revised 21 Aug 2012; accepted 21 Aug 2012; published 31 Aug 2012

stronger provided the A_{21} mode exists. We therefore consider only the even-odd transition in the following computations. We note that the contrast in acoustic material properties for the As_2S_3-SiO_2 system is much larger than for the electromagnetic properties, and higher-order acoustic modes will exist for any geometry that supports a higher-order EM mode.

The intensity of the acoustic field generated by the two pumps depends on the initial pump powers $P_1(0)$ and $P_2(0)$. However, it has been observed [2] that the maximum conversion, and so maximum isolation, of the signal does not occur when the pump powers are equal: this is because equal-power pump beams will generate the largest number of phonons near the front-facet of the waveguide, and the acoustic field will thereafter decay monotonically. Greater conversion efficiency can be achieved by reducing the power of one of the pump beams so that the acoustic field is maximized towards the middle of the waveguide. We therefore first consider the case where the initial pump power $P_2(0)$ is fixed, and we vary the power $P_1(0)$ for a range of waveguide lengths.

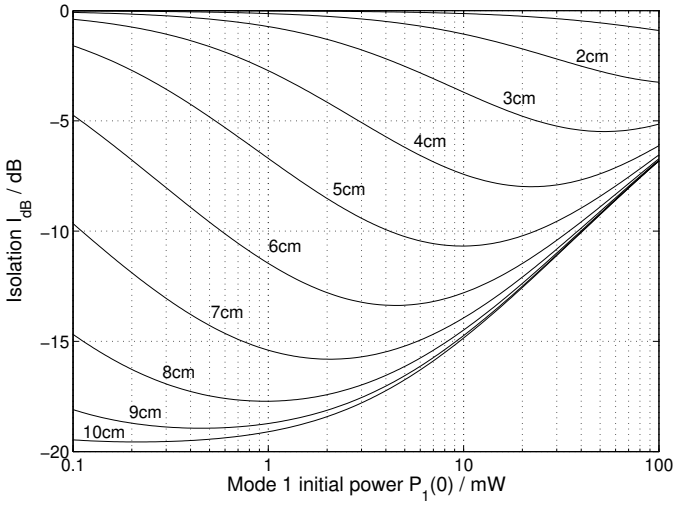

Fig. 5. Computed isolation as a function of initial power in pump 1, as given by Eq. (9). Computed by solving Eq. (5)-(8) with power in pump 2 of $P_2(0) = 400$ mW.

In Fig. 5 we show the isolation I_{dB} as computed from Eq. (9) for waveguide lengths ranging from 2-10 cm. For these computations we have set the wavelength of the pump $\lambda_1 = 1.55$ μm, and λ_2 has been chosen to exactly satisfy the Brillouin resonance condition so as to ensure a maximum phonon generation rate; this results in an acoustic frequency of $\nu(=\Omega/2\pi) = 1.658$ GHz. The signal is chosen such that $\lambda_3 = \lambda_1 + 0.1$ nm, which is sufficiently close to the pump so as to allow phase-matching with the generated phonons but not so close as to make filtering of the final signal difficult. Both pumps and signal are CW: the initial power in the signal is $P_3(0) = 1.0\mu$ W, the initial power in pump 2 is fixed at $P_2(0) =$400 mW and $P_1(0)$ has a maximum value of 100 mW. This choice of powers ensures that the total CW power remains less than 500 mW, which is a conservative estimate for the damage threshold in similar structures. We can see that considerable isolation is achievable even for short waveguide lengths and for modest input powers, with maximum isolation of 19.6 dB occurring for a 10 cm-long waveguide. This level of isolation is of the same order of magnitude as the metres-long air-suspended silica fibre structures studied by Huang and Fan [2].

We can obtain insight into the physics of the mode-conversion process by examining how the

#172916 - $15.00 USD Received 20 Jul 2012; revised 21 Aug 2012; accepted 21 Aug 2012; published 31 Aug 2012

powers $P_k(z)$ change along the waveguide. In Fig. 6 we show the powers at (a) the maximum-isolation predicted by Fig. 5, corresponding to $P_1(0) = 200\ \mu$W and (b) at a higher initial power $P_1(0) = 100$ mW. For high isolation the acoustic field achieves its maximum well within the waveguide, however for more balanced powers the largest values of acoustic field occur at the front of the waveguide and so the overall strength of the mode transition between the signals is reduced.

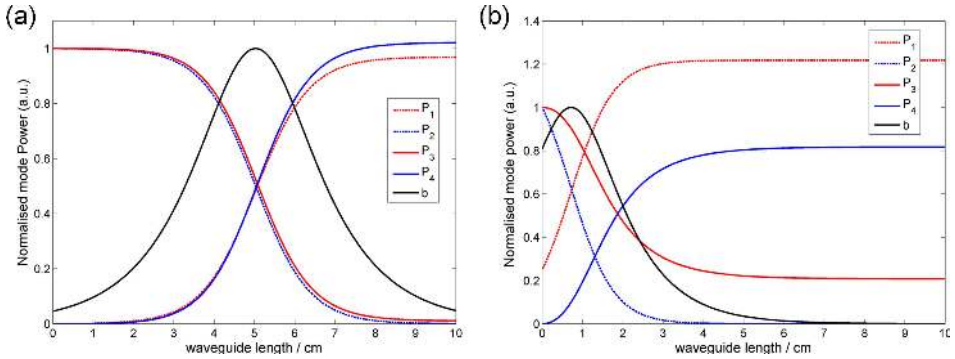

Fig. 6. Power in optical and acoustic modes mode as a function of waveguide length, as computed by solving Eq. (5)-(8) with initial power in pump 2 $P_2(0) = 400$ mW; (a) The maximum-isolation point predicted by Fig. 5, with $P_1(0) = 200\ \mu$ W; (b) Lower isolation point, with $P_1(0) = 100$ mW.

Given that efficient mode conversion is best attained using unbalanced pump powers, and that the total optical power able to be carried in the waveguide will be limited it makes sense to keep the total input power constant $P_0 = P_1(0) + P_2(0)$ and compute the maximum isolation achievable. We show this in Fig. 7, in which we choose waveguide lengths of $z_{\max} = 5$ cm and $z_{\max} = 10$ cm. We see from these results that isolation of > 30 dB can be achieved using a total power of ~ 1 W in a 5 cm guide or ~ 0.5 W in a 10 cm guide.

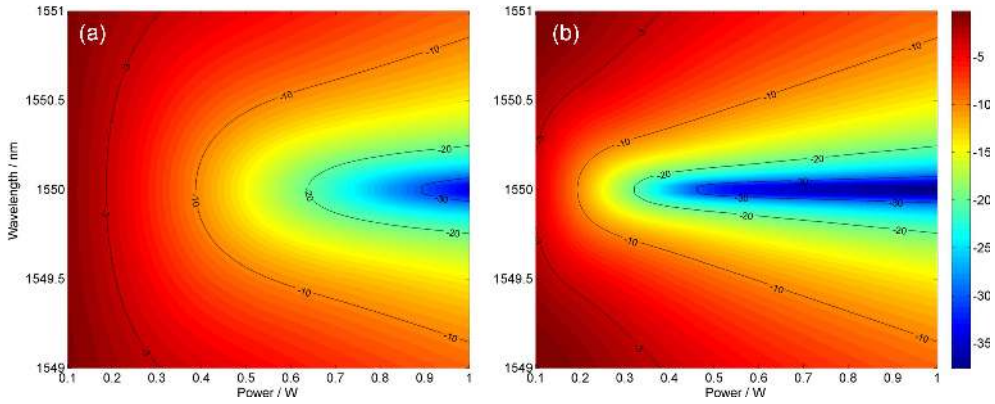

Fig. 7. Maximum isolation, given by Eq. (9), as a function of total power and wavelength, for waveguide lengths of (a) 5 cm and (b) 10 cm. Obtained by numerical solution of (5)-(8).

#172916 - $15.00 USD Received 20 Jul 2012; revised 21 Aug 2012; accepted 21 Aug 2012; published 31 Aug 2012

5. Expanded bandwidth operation by tailoring waveguide dispersion

It can be seen from Fig. 7 that the bandwidth over which significant isolation is achieved is quite small, of the order ~ 0.1 nm. As has been previously noted in the context of long-period gratings [26], the restricted bandwidth is a result of the differences in group velocity between the two optical modes shown in Fig. 3: although appearing almost parallel over the range considered, the slopes of these curves in fact differ by a factor of about 1%, which is enough to cause significant weakening of the acoustically-driven transition in Eq. (8) by increasing the phase mismatch $\Delta\beta$. A natural step is to correct the phase mismatch by tailoring the dispersion of the waveguide modes so that the group velocities of the fundamental and higher-order modes become equal at the operating frequency [3, 26]. Tuning the dispersion is made easier by the difference in fields between the fundamental and higher-order modes, shown in Fig. 3: a localized change in refractive index will affect one mode more than the other. In Fig. 8 we

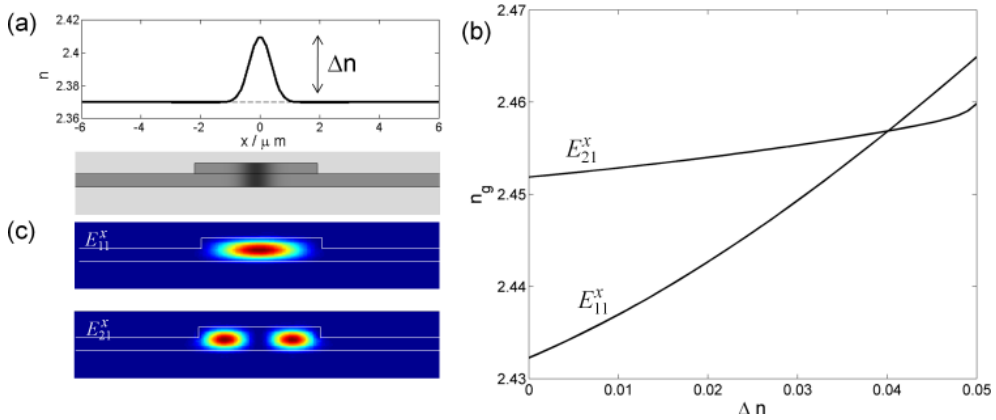

Fig. 8. (a) Cross-section of photo-induced perturbation across the chalcogenide rib; (b) Group index of the optical modes as a function of perturbation height; (c) Mode fields for the first two modes with Δn = 0.04.

examine the effect of a Gaussian index modulation, such as can be photo-induced across the chalcogenide rib [27, 28]. The region of perturbation must be such that the fundamental mode is strongly affected but the higher-order mode is not; for the sake of simplicity we keep the $1/e-$width of the modulation fixed at 1 μm and adjust the maximum index modulation Δn. The resulting change in the group index of each mode is shown in Fig. 8(b), in which we see that the group velocities of the E_{11}^x and E_{21}^x modes are changed at different rates, and become equal when $\Delta n = 0.04$. We note that this is only one of many ways in which the waveguide parameters can be adjusted: others include the inclusion of a high-index material within a slot in the centre of the rib, or the creation of a central 'hat' on the upper rib surface.

With the group velocities matched, we now examine the effect on the bandwidth of the device. As shown in Fig. 9, the bandwidth is dramatically increased: 20 dB isolation can be achieved for a 10 cm device with 0.5 W of total power over a bandwidth of $\Delta\lambda = 25$ nm. The isolation can be increased to 30 dB of isolation with higher powers. It can also be seen that the perturbation creates a second region of group-velocity matching between the two modes at a wavelength of approximately 20 nm higher than the pump. This increase in bandwidth comes at a small cost to the absolute isolation achievable: as can be seen in Fig. 9(a), the maximum isolation for 1 W of power in a 5cm waveguide is now ~ 23 dB, as opposed to more than 30 dB for the non-dispersion-tuned case (Fig. 7). The reason for this is that the perturbation concentrates the mode fields more in the centre of the waveguide (see Fig. 8(c)), thereby reducing the

#172916 - $15.00 USD Received 20 Jul 2012; revised 21 Aug 2012; accepted 21 Aug 2012; published 31 Aug 2012

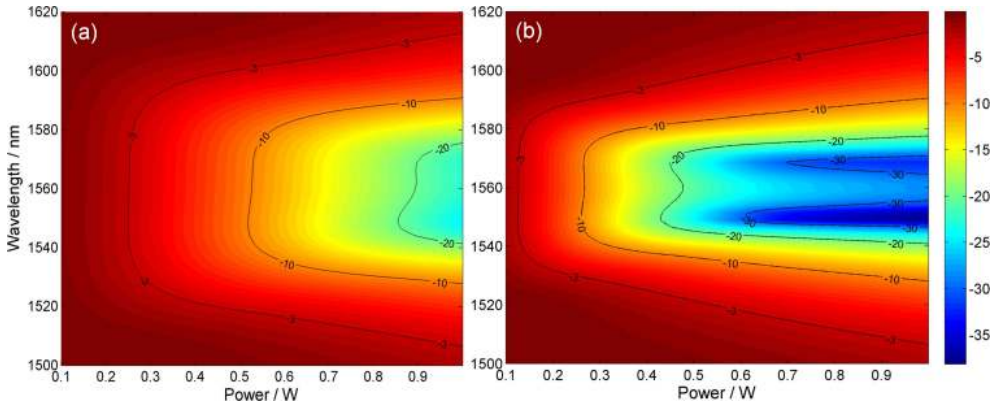

Fig. 9. Maximum isolation I_{dB} for waveguide with v_g-matched modes with lengths of (a) 5 cm and (b) 10 cm, showing broadband operation. Note that the wavelength scale is ~ 60 times larger than for the non-dispersion-tuned waveguide (Fig. 7).

overlap with the acoustic field.

6. Discussion

Any isolation scheme is based on a breaking of reciprocity, or time-reversal symmetry. This can be induced through one of three mechanisms: an intrinsic magnetic response in the material, a nonlinear response, or direct temporal modulation of the refractive index of the material, the latter of which is in essence the approach discussed here. While the use of two auxiliary pump fields may seem overly complicated for an integrated device, there are a number of advantages to the scheme presented here. First, our material system has been demonstrated in a large number of photonic applications and avoids any magnetic elements which are not easily compatible with standard platforms. Further, although the isolation depends on the power in the two pump modes, it is independent of the power of the signal. This is essential for a versatile generic device, and is a significant advantage over nonlinear isolation schemes. We note that, because the signal can be very weak, it will remain unaffected by other $\chi^{(3)}$ nonlinearities in the system: because of the narrow linewidth of the pump modes (less than the Brillouin linewidth), the only effect of these nonlinearities will be to induce a small change in effective index of the pump modes, and this will have a negligible effect on the isolation of the device. Finally, the strong isolation is a direct result of the ability to induce SBS on length scales compatible with on-chip integration, and we can leverage the rapidly growing research effort in SBS-based technologies of all kinds. While we have performed our analysis for chalcogenide glass, recent predictions of photo-elastic effects in silicon [21] suggest that our approach might be suitable for CMOS platforms which would further enhance its appeal and ease of realisation.

It is worth commenting briefly on the effect of imperfections and loss in the device, such as insertion loss, propagation loss, imperfect couplers for the pump modes, and imperfect filtering of the higher-order mode. We note that the first three of these effects are reciprocal, in the sense that they will affect signals propagating in both directions equally. So, while the insertion loss will change the output signal power, as well as the pump powers required to achieve a given isolation, it will not affect the difference I_{dB} between the isolated and non-isolated signals. The effect of waveguide propagation loss α, which may arise due to roughness or material imperfections, will also affect signals propagating in both directions approximately equally; the main effect of propagation loss will be to reduce the power in the pump modes, resulting in a reduc-

#172916 - $15.00 USD Received 20 Jul 2012; revised 21 Aug 2012; accepted 21 Aug 2012; published 31 Aug 2012

tion of the physical length L of the waveguide to an effective length $z_{\max} = (1-\exp(-\alpha L))/\alpha$. Similarly, an imperfect coupler for the pump mode at ω_2 will lead to siphoning of both forward and backward-propagating signals into the pump waveguide at equal rates, because at this section of the waveguide both signals are in the fundamental mode. This will lead to a reduction in the absolute power in the signal but will leave the isolation unchanged. However, a mode-filter will act differently on the signals in the forward and backward propagating directions: an imperfect mode-filter will allow some of the converted signal into the single-mode waveguide at the right-hand-side of Fig. 1, resulting in a reduction in isolation attainable by the device. Structural engineering of mode-filters and couplers [18] will allow the design of devices with isolation to within a given tolerance of the theoretical maximum.

7. Conclusion

We have shown that significant isolation (> 20 dB) can be achieved using SBS in chalcogenide rib waveguides of moderate length. These waveguides can be tuned post-fabrication so as to increase the bandwidth of these devices to several tens of nanometres. These devices can also be used to achieve on-chip conversion to high-order waveguide modes.

Acknowledgments

This work was supported by the Australian Research Council (ARC) through its Discovery grant (DP1096838), Federation fellowship (FF0776056), and Center of Excellence CUDOS (project number CE110001018) programs, and by the U.S. Department of Defense through AFOSR/AOARD (grant #FA23861114030).

#172916 - $15.00 USD Received 20 Jul 2012; revised 21 Aug 2012; accepted 21 Aug 2012; published 31 Aug 2012